



# Simulating the mechanics of sea ice using the discrete element method



Samuel P. Bateman<sup>a,\*</sup>, Mark D. Orzech<sup>b</sup>, Joseph Calantoni<sup>a</sup>

<sup>a</sup> Marine Geosciences Division, U.S. Naval Research Laboratory, Stennis Space Center, MS 39529, USA

<sup>b</sup> Oceanography Division, U.S. Naval Research Laboratory, Stennis Space Center, MS 39529, USA

## ARTICLE INFO

### Article history:

Received 5 December 2018

Revised 17 May 2019

Accepted 29 June 2019

Available online 3 July 2019

### Keywords:

Sea ice

Discrete element method

## ABSTRACT

We developed a technique using the discrete element method (DEM) to simulate the fracture mechanics of ice under flexural, compressive, and tensile loading. In the simulations, virtual blocks of ice are created through a multistep process. First, identical spheres are settled into a random packing. Then, a force network is established at the contact points between spherical elements, which are subsequently replaced by their representative Voronoi volumes. The results of three different sets of tests suggest that the strength of the simulated ice was well characterized using a linear function of the free parameters for the critical bond normal and shear stresses. Additionally, in the flexural strength tests the ratio of the ice thickness to the diameter of the spheres was shown to be sensitive for values less than 4.5, suggesting that a minimum number of bonds was necessary to produce robust estimates for the flexural strength. Overall, the results indicate that the simulations may be calibrated to match the strength properties of various types of ice found in the marginal ice zone (MIZ). The DEM simulations developed here may be used in larger scale models to directly incorporate the effects of ice break up on water waves in the MIZ.

Published by Elsevier Ltd.

## 1. Introduction

Sea ice consists of varying combinations of pure ice, salty brine, gas inclusions, and occasionally some types of solid salts. Because it can develop under a range of environmental conditions, sea ice can have different grain structures. Its variable composition and growth patterns cause it to exhibit a range of material strength properties, which can also change over time as surrounding temperatures and solar radiation vary. Recently frozen seawater that has begun to consolidate is generally known as “new ice” and may also be given names such as frazil, slush, grease, pancakes, or nilas depending on composition and material properties. It tends to be relatively malleable and flexible, with high salinity of 10 to 15 practical salinity units (psu) and thickness of O(10 cm). First-year sea ice, formed within the past year, has an average salinity of 4 psu to 6 psu and a thickness generally not larger than 2 m. So-called “old ice”, which has existed for two or more years, is almost salt-free and can reach thicknesses of over 10 m [1].

The material strength properties of first-year and older sea ice have been measured with a range of laboratory experiments, in which vertical and/or horizontal ice sections are subjected to ten-

sile, compressive, or bending stress. A very low ambient temperature ( $< -24^\circ$ ) is generally maintained to minimize brine drainage [e.g., [2–4]]. A compilation of stress test results [1] provides realistic ranges for the fracture strength of sea ice under each different type of stress. Depending on porosity and temperature, the tensile strength of first-year ice varies from 0.2 MPa to 0.8 MPa. Flexural strength can range from very small values (O(100 kPa)) up to 2 MPa or more, depending on ice salinity and temperature. The strength of sea ice is greatest in compression and can even exceed 10 MPa for very high loading rate and low temperature, although values are closer to 1 MPa for more typical conditions.

The discrete element method (DEM) was originally used to model sea ice as clusters of contiguous platelike elements, each roughly the size of smaller individual ice floes [5,6]. Initial research goals focused on understanding and predicting ice buildup through ridging as larger plates were pushed into the shoreline by ocean currents. More recent work represented the ice floes themselves as composites of smaller elements, initially in two dimensions (2D) [7] and later in three dimensions (3D) [8,9]. The recent approach facilitated the investigation of small-scale flexing and fracture of individual floes as well as their effects on ocean surface waves propagating through more realistic representations of Arctic marginal ice zones [10].

The goal of the effort described herein is to accurately model the average strength properties of first-year sea ice with a 3D DEM

\* Corresponding author.

E-mail address: [sam.bateman@nrlssc.navy.mil](mailto:sam.bateman@nrlssc.navy.mil) (S.P. Bateman).

simulation. As with other recent work, virtual ice blocks in our study are composed of large collections of individual, smaller elements, each of which is bonded to its neighbors under a prescribed elastic bonding regime [11,12]. In contrast to the earlier efforts, this analysis seeks to calibrate and validate the dynamic behavior of virtual DEM ice blocks by direct comparison to that of actual sea ice, as measured in a series of flexural, compressive, and tensile stress tests. To determine and validate the optimal bonding parameters, blocks were subjected to virtual stress tests, applying and gradually increasing tension, compression, or bending stress until the block fractures. The inter-element bond strength limits were adjusted until the critical failure stress determined for the block in each test falls within the ranges previously observed [1]. Below we describe the techniques used to construct, configure, and validate virtual sea ice blocks using an open-source DEM model.

## 2. Methods

### 2.1. Ice model

We developed a simulation technique using the open-source discrete element method (DEM) software, LIGGGHTS [13], which is a modified version of the LAMMPS molecular dynamics (MD) software [14], to simulate the fracture mechanics of ice floes under flexural, compressive, and tensile loading. In the simulations, each ice floe is initially created by settling a large number of distinct spherical ice elements into a random packing. Soft sphere contacts between ice elements facilitate nearest neighbor interactions through distinct contact and bond forces. The bond between a pair of ice elements will break when the bond stress exceeds a critical threshold. Once a force network is established the spherical ice elements are replaced with their representative Voronoi volumes. The equations of motion for each ice element are solved simultaneously using a velocity Verlet time integration. The translational and rotational equations of motion for an ice element,  $i$ , may be written as,

$$\rho_i V_i \frac{du_i}{dt} = F_i, \quad (1)$$

and

$$0.1 \rho_i V_i \frac{d\omega_i}{dt} = \tau_i, \quad (2)$$

respectively, where  $\rho_i$  is the density of the ice element,  $V_i$  is the volume of the Voronoi cell containing the ice element,  $u_i$  is the velocity of the ice element,  $F_i$  is the total force acting on the ice element,  $\omega_i$  is the rotational velocity, and  $\tau_i$  is the total torque acting on the ice element. Spherical elements are initially used to create the bond network within the ice floe; however, each ice element effectively represents a small non-spherical “chunk” of the entire ice floe through the use of the Voronoi cell and volume. Consequently, the initial spherical volume ( $\frac{\pi}{6} D^3$ ) of the ice element is later replaced with the volume of its Voronoi cell,  $V_i$ .

Each pair of neighboring ice elements may interact through contact and bond forces. The contact force between two ice elements is divided into normal and tangential components. The normal component of the contact force is computed using a linear spring and a velocity-dependent damping term (dashpot),

$$F_{g,n} = k_{g,n} \delta_n - \gamma_n \frac{d\delta_n}{dt}, \quad (3)$$

where  $F_{g,n}$  is the magnitude of the normal contact force,  $k_{g,n}$  is the normal contact spring constant,  $\delta_n = D - |\vec{n}|$  is the overlap distance at the contact point,  $\gamma_n$  is the normal contact damping coefficient,

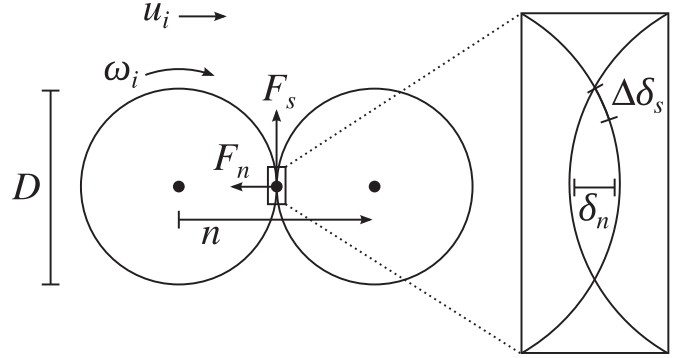


Fig. 1. Interaction between two ice elements.

$D$  is the particle diameter,  $\vec{n} = \vec{x}_j - \vec{x}_i$  is the normal vector between particle centers (pointing from particle  $i$  to  $j$ ), and  $\vec{x}_i$  and  $\vec{x}_j$  are the locations of the particle centers. Contact between neighboring ice elements exists when the surfaces of the spheres are overlapping, i.e.  $\delta_n > 0$  (see Fig. 1).

The tangential component of the contact force is history-dependent and incrementally updated by an amount proportional to the tangential displacement at the contact point,

$$\vec{F}_{g,s}(t) = \vec{F}_{g,s}(t - \Delta t) + k_{g,s} \Delta \delta_s, \quad (4)$$

where  $\vec{F}_{g,s}(t)$  is the tangential component of the contact force vector at time  $t$  (i.e. the current simulation timestep),  $\vec{F}_{g,s}(t - \Delta t)$  is the tangential component at time  $t - \Delta t$  (i.e. the previous simulation timestep), and  $k_{g,s}$  is the tangential contact spring constant.  $\Delta \delta_s$  is the incremental change in the tangential displacement vector along the surface of the particles (see Fig. 1) and may be written as,

$$\Delta \delta_s = \Delta t (\vec{u}_{rel,rot} + \vec{u}_{rel,tan}), \quad (5)$$

where

$$\vec{u}_{rel,rot} = \hat{n} \times \left[ \frac{\vec{\omega}_i}{2} (D_i - \delta_n) + \frac{\vec{\omega}_j}{2} (D_j - \delta_n) \right] \quad (6)$$

is the relative rotational motion of the particles, and

$$\vec{u}_{rel,tan} = (\vec{u}_j - \vec{u}_i) - [(\vec{u}_j - \vec{u}_i) \cdot \hat{n}] \hat{n}, \quad (7)$$

is the relative translational motion of the particles, and  $\hat{n} = \vec{n}/|\vec{n}|$  is the normal unit vector. The tangential component of the contact force is scaled according to a Coulomb friction law  $|\vec{F}_{g,s}(t)| < \mu F_{g,n}$ , where  $\mu$  is the friction coefficient of ice.

The normal and tangential spring constants are estimated using the material properties of the ice as  $k_{g,n} = ED$  and  $k_{g,s} = ED/[2(1 + \nu)]$ , where  $E$  is Young's modulus and  $\nu$  is Poisson's ratio. The total contact force on particle,  $i$ , from the interaction with particle,  $j$ , is the sum of the normal and tangential components. The contact force on particle  $j$  is simply the equal and opposite force,

$$\vec{F}_{g,i} = -\vec{F}_{g,j} = -F_{g,n} \hat{n} + \vec{F}_{g,s}(t). \quad (8)$$

After the particles are settled into a packing, each pair of contacting neighbors forms a bond. As long as the bond is not yet broken (i.e., the critical bond stress has not been exceeded), the particles interact through bond forces. Note that this interaction continues when the particles are separated by a small distance so they are no longer in contact, as long as the distance is not so large as to cause enough stress to break the bond.

The bond force between two particles is divided into normal and tangential components. The normal component is computed using a linear spring,

$$F_{b,n} = k_{b,n} A_b |\delta_n|, \quad (9)$$

where  $F_{b,n}$  is the magnitude of the normal component of the bond force,  $k_{b,n}$  is the normal bond spring constant,  $A_b = \frac{1}{4}\pi D^2$  is the bond cross-sectional area. Note that  $\delta_n$  may be negative if the particles are not in contact. For the tangential component, we incrementally update the history-dependent force by an amount proportional to the tangential displacement,

$$\vec{F}_{b,s}(t) = \vec{F}_{b,s}(t - \Delta t) + k_{b,s} A_b \Delta \vec{\delta}_s, \quad (10)$$

where  $\vec{F}_{b,s}$  is the tangential component of the bond force and  $k_{b,s}$  is the tangential bond spring constant. Similarly to the contact force, we compute the value at the current timestep ( $t$ ) from the value at the previous timestep ( $t - \Delta t$ ).

The normal and tangential spring constants are computed as  $k_{b,n} = E/D$  and  $k_{b,s} = E/[2(1 + \nu)D]$ , respectively. The total bond force on particle  $i$  (and the opposing force on particle  $j$ ) is the sum of the normal and tangential components,

$$\vec{F}_{b,i} = -\vec{F}_{b,j} = F_{b,n} \hat{n} + \vec{F}_{b,s}(t). \quad (11)$$

The bond angle between two particles is updated incrementally from their relative rotation as,

$$\vec{\theta}(t) = \vec{\theta}(t - \Delta t) + \Delta t [\omega_j - \omega_i], \quad (12)$$

$$\vec{\theta}_n = (\vec{\theta}(t) \cdot \hat{n}) \hat{n}, \quad (13)$$

$$\vec{\theta}_s = \vec{\theta}(t) - \vec{\theta}_n, \quad (14)$$

where  $\vec{\theta}$  is the bond angle, and  $\vec{\theta}_n$  and  $\vec{\theta}_s$  are the “twisting” and “bending” angles respectively. From these, we can compute the bond moments as  $\vec{M}_n = -k_{b,n} J \vec{\theta}_n$ ,  $\vec{M}_s = -k_{b,s} l \vec{\theta}_s$ ,  $I = A_b D^2 / 16$ , and  $J = A_b D^2 / 8$ , where  $\vec{M}_n$  and  $\vec{M}_s$  are the twisting and bending moments of the parallel bond, respectively, and  $J$  and  $I$  are the area moments of inertia of the circular bond cross-section along the normal and tangential axes, respectively. The normal and shear stress on the bond is then computed from the bond forces and moments,

$$\sigma_n = \frac{F_{b,n}}{A_b} + \frac{|\vec{M}_s| D}{2I}, \quad (15)$$

and

$$\sigma_s = \frac{|\vec{F}_{b,s}|}{A_b} + \frac{|\vec{M}_n| D}{2J}, \quad (16)$$

respectively. If either the normal or shear bond stress exceeds a critical threshold ( $\sigma_n > \sigma_{crit,n}$  or  $\sigma_s > \sigma_{crit,s}$ ), the bond breaks and bond forces and moments are no longer computed between the two particles. Additionally, the tangential contact and bond forces and the bond moments contribute to the torque on both particles  $i$  and  $j$  as,

$$\vec{\tau}_i = \vec{\tau}_j = [\hat{n} \times (\vec{F}_{g,s} + \vec{F}_{b,s})] \frac{D - \delta_n}{2} + \vec{M}_n + \vec{M}_s. \quad (17)$$

## 2.2. Strength test simulations

We designed a series of strength test simulations to evaluate the bulk properties of our simulated ice as compared to the experimentally-measured properties of real sea ice. We focused our tests on the bulk properties of the ice for flexural, compressive, and tensile strength. The “strength” of the ice is defined as the fracturing stress, i.e. the maximum stress that can be loaded onto a block of ice before it fractures. To measure the strength in the laboratory,

**Table 1**  
Simulation parameters.

Parameter	Symbol	Value
Young's modulus	$E$	9 GPa
Poisson's ratio	$\nu$	0.3
Damping coefficient	$\gamma_n$	100 kg.s <sup>-1</sup>
Friction coefficient	$\mu$	0.05
Ice density	$\rho$	920 kg.m <sup>-3</sup>
Ice block length	$l$	1 m
Particle diameter	$D$	2 cm
Strain rate	$\dot{\epsilon}$	1e-3 s <sup>-1</sup>
Critical normal stress	$\sigma_{crit,n}$	0.5 MPa–2.0 MPa
Critical shear stress	$\sigma_{crit,s}$	0.5 MPa–2.0 MPa

typically a block of ice will have a load applied to it, increasing until the ice fractures. The strength is then measured as the peak of the stress-strain curve observed during the loading process.

To perform our strength test simulations, we chose the conditions and setup to match the recommendations of [15] for laboratory experiments (Table 1). We observed the stress-strain curve until fracture of our simulated ice occurred. The results allow us to evaluate the sensitivity of our model parameters. Each of the three different sets of tests performed for flexural, compressive, and tensile strength are described below.

### 2.2.1. Flexural strength tests

We simulated the three-point loading method of flexural strength testing. In the three-point loading method, a long, thin beam of ice is placed on top of two points supporting both ends, while a third point presses down in the middle above the ice block. The middle point above provides the “loading”, and also acts as a force measurement device. By prescribing the force applied to the ice beam, and using simple beam theory, we can calculate the stress in the ice block upon fracture and, thus, estimate the flexural strength.

A flexural strength test simulation proceeds in several steps. In the first step, “packing”, particles are created at non-overlapping points inside a container with thickness  $L_z = 0.1l$  and width  $L_y = 0.2l$ , where  $l$  is the separation distance between the two points where the ice beam will rest during loading (Fig 2(a)). The particles then fall under gravity in the  $-x$  direction until they settle into a random packed configuration with a packing fraction of between 0.6 and 0.63. There are no inter-particle bonds during the “packing” step; the particles only interact through contact forces. After the particles are settled, they fill a box with length  $2l$ . In the next step, “freezing”, the particles between  $0.25l < x < 1.75l$  form bonds

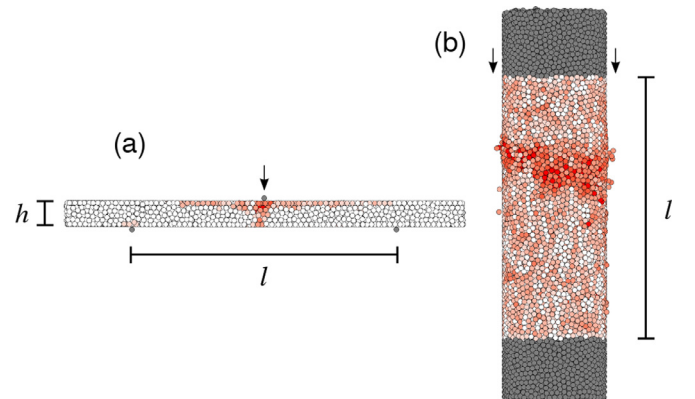


**Fig. 2.** Visualizations of (a) flexural and (b) compressive strength test simulations, at the instant of fracture during the “loading” phase. Each ice particle is colored by how many of its inter-particle bonds have been broken, from white (no bonds broken) to red (6 bonds broken). Grey particles indicate (a) points and (b) plates. (For interpretation of the references to colour in this figure legend, the reader is referred to the web version of this article.)

with all of their contacting neighbors, which creates a mostly rigid block of ice with length  $L_x = 1.5l$  in the center of the container. The extra particles on the ends (where  $x < 0.25l$  or  $x > 1.75l$ ) are discarded to eliminate wall effects.

In the final step, “loading”, three lines of particles are placed around the ice beam (the “points” in the three-point method). Two lines are placed directly below the beam at positions  $x = 0.5l$  and  $x = 1.5l$ . The two lines are made permanently fixed in the simulation. The third, “loading” line is placed directly above the beam at position  $x = l$ . The loading line has a prescribed motion downward through the ice beam, allowing us to apply a constant strain rate during the flexural strength test. Prior to loading, all the container walls are eliminated and gravity is applied in the  $-z$  direction, so that the ice beam rests on the supporting lines while being fractured by the loading line of particles. Following the experimental setup described by [15], we can use beam theory to calculate an “index” flexural strength  $\sigma_F$  from our simulations as

$$\sigma_F = \frac{3}{2} \frac{Fl}{bh^2}, \quad (18)$$

where  $\sigma_F$  is the flexural strength,  $F$  is the force applied by the loading point (line of particles) at the time of fracture,  $l$  is the distance between supporting points,  $b = 0.2l$  is the beam width, and  $h = 0.1l$  is the beam thickness (Fig 2(a)).

### 2.2.2. Compressive and tensile strength tests

To estimate compressive and tensile strengths, we performed simulations using cylindrical ice blocks under either compressive or tensile loading. The simulations followed a similar design to the experimental setup for compressive uniaxial strengths tests performed in the laboratory (e.g. [15]). In the experimental setup, a cylindrical block of ice is fitted vertically between two plates on the top and bottom. The bottom plate is held fixed, while compressive force is applied by the top plate pushing down on the ice. The total force applied to the ice at every time step is recorded. Once the ice block fractures, the maximum force and the surface area of the plates are used to calculate the pressure at which the ice fractures, i.e. the compressive strength.

The simulation setup for compressive/tensile strength tests proceeds in three steps. In the “packing” step, particles are created inside a cylinder with radius  $R_{cyl} = 0.2l$ , where  $l$  is the distance between the top and bottom plates (Fig 2(b)). The particles fall under gravity in the  $-z$  direction and settle into a random packed configuration with no inter-particle bonds, filling the cylinder up to height  $1.5l$ .

In the next step, “freezing”, the particles at  $z < 0.25l$  are designated as the bottom plate, and the particles at  $z > 1.25l$  are designated as the top plate. In tensile strength tests during “freezing”, both ice and plate particles form inter-particle bonds with each of their contacting neighbors. In compressive strength tests during “freezing”, only ice particles (not plate) form inter-particle bonds.

In the final step, “loading”, the bottom plate remains permanently fixed during the simulation, while the top plate is moved at a constant velocity, vertically, either down (compressive loading) or up (tensile loading). After the ice block fractures, we estimate the compressive strength,  $\sigma_C$ , or tensile strength,  $\sigma_T$ , as,

$$\sigma_C = \frac{F_C}{\pi R_{cyl}^2} \quad \text{or} \quad \sigma_T = \frac{F_T}{\pi R_{cyl}^2}, \quad (19)$$

where  $F_C$  is the compressive force and  $F_T$  is the tensile force applied at the time of fracture. The denominator is the “surface area” of the top and bottom plates calculated using  $R_{cyl}$ , the radius of the cylindrical ice block.

## 3. Results

We found the flexural, compressive, and tensile strength of our simulated ice (estimated as the fracturing stress) was well described by a linear combination of the free model parameters, the critical bond normal ( $\sigma_{crit,n}$ ) and shear ( $\sigma_{crit,s}$ ) stresses,

$$\sigma = A[\sigma_{crit,n}] + B[\sigma_{crit,s}] - C[\min(\sigma_{crit,n}, \sigma_{crit,s})]. \quad (20)$$

Optimal values for the three coefficients are provided in Table 2, along with the correlation ( $R^2$ ) for each case. Results are plotted in Fig. 3, showing the linear relation between ice strength and the critical bond stresses, as one (either  $\sigma_{crit,n}$  or  $\sigma_{crit,s}$ ) is allowed to vary while the other remains constant, or they both vary equally ( $\sigma_{crit,n} = \sigma_{crit,s}$ ).

In the simulations where  $\sigma_{crit,n} = \sigma_{crit,s}$ , (20) reduces to a single line, which is shown in Fig. 3 as the solid line. In the simulations where  $\sigma_{crit,s}$  varies and  $\sigma_{crit,n}$  is set to a constant 1.0 MPa (dashed lines) or 1.5 MPa (dotted lines) (Fig. 3(a–c)), and in the

**Table 2**  
Optimal values for coefficients in (20).

Strength	A	B	C	$R^2$
Flexural	0.1895	0.0545	0.5911	0.8947
Compressive	0.1058	0.0240	0.5591	0.9668
Tensile	0.3010	-0.0102	0.3220	0.9628

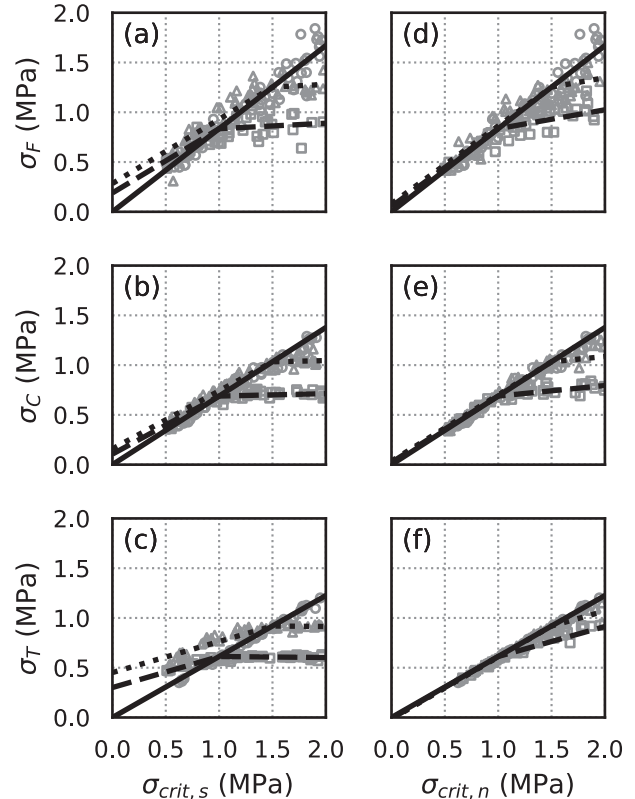


**Fig. 3.** Results of 724 simulations to measure the fracturing strength of ice under flexural, compressive, or tensile loading. (a–c) The points show the strengths of modeled ice for series of simulations where the critical bond shear stress,  $\sigma_{crit,s}$ , was varied, while the critical bond normal stress,  $\sigma_{crit,n}$ , was either set to be equal to the shear stress,  $\sigma_{crit,n} = \sigma_{crit,s}$  (circles), or was set to a constant value  $\sigma_{crit,n} = 1.0$  MPa (squares) or  $\sigma_{crit,n} = 1.5$  MPa (triangles). The lines correspond to linear fits of (20) to the simulation results for the simulations where  $\sigma_{crit,n} = \sigma_{crit,s}$  (solid),  $\sigma_{crit,n} = 1.0$  MPa (dashed), and  $\sigma_{crit,n} = 1.5$  MPa (dotted). (d–f) Simulations where  $\sigma_{crit,n}$  was varied, and  $\sigma_{crit,s}$  was either set to be equal to the normal stress,  $\sigma_{crit,s} = \sigma_{crit,n}$  (circles, solid), or was set to a constant value  $\sigma_{crit,s} = 1.0$  MPa (squares, dashed) or  $\sigma_{crit,s} = 1.5$  MPa (triangles, dotted).

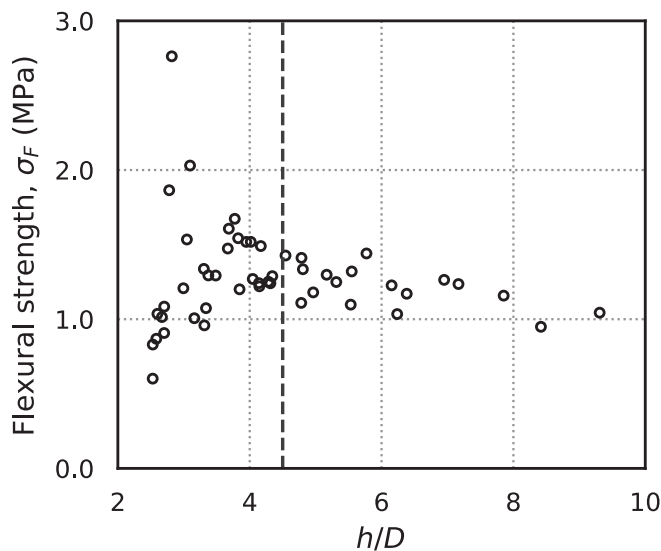


**Fig. 4.** Results of 50 simulations to measure the dependency of ice flexural strength on the ratio of ice block thickness  $h$  to particle diameter  $D$ . In all simulations, critical bond normal and shear stresses were set to  $\sigma_{crit,n} = \sigma_{crit,s} = 1.5$  MPa.

simulations where  $\sigma_{crit,n}$  varies and  $\sigma_{crit,s}$  is set to a constant 1.0 MPa (dashed lines) or 1.5 MPa (dotted lines) (Fig. 3(d–f)), (20) becomes two lines with different slopes. The two lines roughly intersect at a point, where the varying critical bond stress is the same as the constant critical bond stress. To the left of the intersection point, the min term in (20) varies, and to the right of the intersection point, the min term is constant, resulting in the two different slopes.

#### 4. Discussion and conclusions

We used the DEM software package, LIGGGHTS, to construct virtual ice blocks and perform simulations to estimate the bulk mechanical properties of the simulated ice, including the flexural, compressive, and tensile strength. The DEM allowed us to simulate the ice as a collection of bonded particles that interact through contact and bond forces, with bonds that break when the inter-particle stress exceeds a critical threshold. Our results suggest that the strength of our simulated ice was primarily dependent on the critical bond normal and shear stresses and fits well with a linear function of those free model parameters. Other variables such as Young’s modulus and Poisson’s ratio have little-to-no impact on the ice strength in our simulations across the ranges typical for sea ice.

In Fig. 3(d–f), in the region with  $\sigma_{crit,n} < 1.0$  MPa, the fitted lines overlapped each other, even for different values of the constant  $\sigma_{crit,s}$ . However, in Fig. 3(a–c), in the region with  $\sigma_{crit,s} < 1.0$  MPa, the fitted lines did not overlap. The difference suggests the critical bond normal stress,  $\sigma_{crit,n}$ , is more important than the critical bond shear stress,  $\sigma_{crit,s}$ , in determining the flexural, compressive, and tensile strength of the ice. The importance of  $\sigma_{crit,n}$  was also supported by the relatively high value of the fitting coefficient  $A$  compared to  $B$  in (20) (Table 2). The difference between  $A$  and  $B$  was even greater for the tensile strength than for flexural or compressive strength, indicating an even greater dependence on  $\sigma_{crit,n}$  over  $\sigma_{crit,s}$  for tensile strength.

The flexural strength (Fig. 3a, d) contained more scatter than the compressive strength (Fig. 3b, e) or tensile strength (Fig. 3c, f) in the regions  $\sigma_{crit,n} > 1.0$  MPa and  $\sigma_{crit,s} > 1.0$  MPa. Despite the scatter, the fitted lines for flexural strength (Table 2) have a correlation coefficient  $R^2$  of almost 0.9. Also, the simulated flexural strengths at those high values of critical bond stress are larger than

typical flexural strengths of sea ice estimated from experimental measurements (e.g. [16]), so while fitting model parameters to values of flexural strength larger than 1.0MPa is difficult because of scatter, those values are less likely to occur in nature. Additionally, we performed a suite of simulations to investigate the sensitivity of other simulation parameters. Young’s modulus  $E$  varied in the range 1.0 GPa to 10.0 GPa, Poisson’s ratio  $\nu$  varied in the range 0.2 to 0.5, and the friction coefficient  $\mu$  varied in the range 0.05 to 0.1. None of the simulation parameters  $E$ ,  $\nu$ , or  $\mu$  were found to have a significant effect on the fracturing strength of the simulated ice in flexural, compressive, or tensile strength tests.

The strength of the ice was found to be sensitive to the choice of the particle diameter  $D$ . Fig. 4 shows the results of a series of simulations where the ratio of the ice block thickness  $h$  to the particle diameter  $D$  was varied in the range 2.5 to 10.0. In the region where  $h/D > 4.5$ , the flexural strength was mostly constant and was consistent with the results shown in Fig. 3(a, d). In the region where  $h/D < 4.5$ , the flexural strength became scattered and inconsistent. The scattering suggests that when  $h/D < 4.5$ , the “network” of inter-particle bonds is either too anisotropic or too inhomogeneous to distribute the stress among the particles in the packing, resulting in the ice block fracturing at unrealistic stresses. Above  $h/D > 4.5$ , the inter-particle bonds are homogeneous enough to efficiently distribute the applied stress throughout the ice block. Previous work [17] confirms the threshold value of  $h/D = 4.5$  as appropriate in a random pack for reducing the noise level of continuum properties such as the inter-particle bond network homogeneity. The analysis results may be used to calibrate the critical bond stresses in the model for realistic simulation of various types of ice found in marginal ice zones.

#### Conflict of interest

None.

#### Acknowledgments

We thank the anonymous reviewers for their comments and suggestions, which significantly improved this manuscript. This work was supported under base funding to the U.S. Naval Research Laboratory from the Office of Naval Research. This work was supported in part by a grant of computer time from the DoD High Performance Computing Modernization Program (HPCMP) on the Cray XC40 system “excalibur” at ARL DSRC and the Cray XE6 system “garnet” at the ERDC DSRC.

#### References

- [1] G. Timco, W. Weeks, A review of the engineering properties of sea ice, *Cold Reg. Sci. Technol.* 60 (2) (2010) 107–129.
- [2] T. Butkovich, Strength studies of sea ice, Research Report 20, 1956.
- [3] J.R. Menge, K. Jones, The tensile strength of first-year sea ice, *J. Glaciol.* 39 (133) (1993) 609–618.
- [4] P. Moslet, Field testing of uniaxial compression strength of columnar sea ice, *Cold Reg. Sci. Technol.* 48 (1) (2007) 1–14.
- [5] M.A. Hopkins, W. Hibler, G. Flato, On the numerical simulation of the sea ice ridging process, *J. Geophys. Res. Oceans* 96 (C3) (1991) 4809–4820.
- [6] M.A. Hopkins, On the ridging of intact lead ice, *J. Geophys. Res. Oceans* 99 (C8) (1994) 16351–16360.
- [7] Z. Xu, A.M. Tartakovsky, W. Pan, Discrete-element model for the interaction between ocean waves and sea ice, *Phys. Rev. E* 85 (1) (2012) 016703.
- [8] A. Herman, Numerical modeling of force and contact networks in fragmented sea ice, *Ann. Glaciol.* 54 (62) (2013) 114–120.
- [9] A. Herman, Wave-induced stress and breaking of sea ice in a coupled hydrodynamic discrete-element wave–ice model, *Cryosphere* 11 (6) (2017) 2711.
- [10] M.D. Orzech, F. Shi, J. Veeramony, S. Bateman, J. Calantoni, J.T. Kirby, A coupled system for investigating the physics of wave-ice interactions, *J. Atmos. Ocean. Technol.* (2018) (2018).
- [11] J. Tuhkuri, A. Polojärvi, A review of discrete element simulation of ice–structure interaction, *Philos. Trans. R. Soc. A* 376 (2129) (2018) 20170335.

- [12] S. Di, Y. Xue, X. Bai, Q. Wang, Effects of model size and particle size on the response of sea-ice samples created with a hexagonal-close-packing pattern in discrete-element method simulations, *Particuology* 36 (2018) 106–113.
- [13] C. Kloss, C. Goniva, A. Hager, S. Amberger, S. Pirker, Models, algorithms and validation for opensource DEM and CFD-DEM, *Prog. Comput. Fluid Dyn.* 12 (2–3) (2012) 140–152.
- [14] S. Plimpton, Fast parallel algorithms for short-range molecular dynamics, *J. Comput. Phys.* 117 (1) (1995) 1–19.
- [15] J. Schwarz, R. Frederking, V. Gavrillo, I. Petrov, K.-I. Hirayama, M. Mellor, P. Tryde, K. Vaudrey, Standardized testing methods for measuring mechanical properties of ice, *Cold Reg. Sci. Technol.* 4 (3) (1981) 245–253.
- [16] G. Timco, S. O'Brien, Flexural strength equation for sea ice, *Cold Reg. Sci. Technol.* 22 (3) (1994) 285–298.
- [17] J.A. Simeonov, S. Bateman, J. Calantoni, Filter width and uncertainty estimation in continuum modeling of particle phases, *Int. J. Multiph. Flow* 74 (2015) 79–83.